STRUCTURE AND CYCLIC VARIATIONS OF OPEN MAGNETIC FIELDS IN THE SUN

V. N. OBRIDKO and B. D. SHELTING
IZMIRAN, 142092, Troitsk, Moscow Region, Russia

(Received 28 October 1997; accepted 2 March 1999)

Abstract. The structure and variations of open field regions (OFRs) are analyzed against the solar cycle for the time interval of 1970–1996. The cycle of the large-scale magnetic field (LSMF) begins in the vicinity of maximum Wolf numbers, i.e. during the polar field reversal. At the beginning of the LSMF cycle, the polar and mid-latitude magnetic field systems are connected by a narrow bridge, but later they evolve independently. The polar field at the latitudes above 60° has a completely open configuration and fills the whole area of the polar caps near the cycle minimum of local fields. At this time, essentially all of the open solar flux is from the polar caps. The mid-latitude open field regions (OFRs) occur at a latitude of 30–40° away from solar minimum and drift slowly towards the equator to form a typical 'butterfly diagram' at the periphery of the local field zone. This supports the concept of a single complex – 'large-scale magnetic field – active region – coronal hole'. The rotation characteristics of OFRs have been analyzed to reveal a near solid-body rotation, much more rigid than in the case of sunspots. The rotation characteristics are shown to depend on the phase of the solar cycle.

1. Introduction

Coronal holes (CHs) appear as dark regions on X-ray and EUV solar images and as light regions when observed in the He 10830 absorption line. The analysis of EUV images shows that the density and temperature in coronal holes are about half that of the neighboring magnetically closed regions of the corona (Munro and Withbroe, 1972; Withbroe and Wang, 1972). Coronal holes have been shown to occur inside large-scale unipolar regions in the Sun with one predominant polarity of the magnetic field. Proceeding from the potential models computed from magnetic field observations in the photosphere (Altschuler, Trotter, and Orall, 1972; Levine *et al.*, 1977; Pneuman, Hansen, and Hansen, 1978), one can infer that the field lines in CHs are open and escape to interplanetary space, unlike the closed configurations, where the field lines ultimately return to the photosphere. The *Skylab* data, obtained in 1973–1974, revealed near solid-body rotation of coronal holes (Timothy, Krieger, and Vaiana, 1975). The role of CHs as the source of high-speed streams of the solar wind (HSWS) was established in the early 70s (Krieger, Timothy, and Roelof, 1973; Sheeley, Harvey, and Feldman, 1976; Kovalenko, 1983; Veselovsky, 1984; Rozelot, 1983; Obridko *et al.*, 1986). A review of physical conditions in coronal holes was given by Mogilevsky, Obridko, and Shilova (1997).

Solar Physics **187:** 185–205, 1999.

This work is devoted to the study of the structure and cyclic variation of the photospheric open field regions (OFRs). This physical phenomenon is of particular interest as the triggering factor in the occurrence of coronal holes, which are in turn one of the principal elements of the large-scale solar activity. Besides, using magnetic field data and up-to-date calculation techniques, we can study OFRs for a longer time interval than CHs.

Section 2 describes the magnetic field data from several magnetographs and the methods used for calculations. The analysis incorporates CORONAS, *Yohkoh*, and SOHO observations, as well as the data on the high-speed solar wind. In Sections 3 and 4, we discuss the degree of coincidence between OFRs and CHs. They prove to be interchangeable for the purposes of *statistical* analysis, though lacking full similarity. The structure of magnetic field in CHs is considered to show that CHs, as elements of the global field, in many respects resemble sunspots as elements of the local field. Section 5 describes the distribution of OFRs on the Sun depending on the phase of the solar cycle. The distribution pattern is shown to change abruptly from a simply-connected compact region near each pole at the beginning of the cycle to a fragmented filament structure at the maximum of the cycle. These data are used in Section 6 to analyze the OFR rotation characteristics, both on average and as a function of the solar cycle. And finally, in Section 7 our analysis of the cyclic evolution of OFRs reveals two effects. Firstly, a sign reversal in OFRs occurs simultaneously at all latitudes. Secondly, OFRs display two modes of rotation.

2. The Used Data and Calculation Technique

Information on the large-scale solar magnetic field (LSMF) is obtained by direct magnetographic observations of the Sun. Routine observations of these fields began at the end of the 1950s. We have at our disposal several series of observation data. One of them comprises the synoptic charts of photospheric magnetic fields obtained by the R. Howard team at the Mt. Wilson Observatory for the time period August 1959–December 1978 (Carrington rotations 1417–1648). Another series contains the data for January 1975–July 1984 (Carrington rotations 1622–1751) obtained under the surveillance of J. Harvey at the Kitt Peak National Observatory (KPNO). And finally, the third series, which was kindly made available to us by T. Hoeksema, is the observation series from the John Wilcox Observatory of Stanford University. These observations started in May 1976 (Carrington rotation 1641) and continue at present.

We have used all three series in our calculations. To avoid inhomogeneous data, we have reduced them to a single scale by comparing the data in the overlapping time intervals. However, the most reliable and uniform data begin in 1976.

In many problems, to compare CHs and HSWS it is sufficient to use direct observations of the LSMF neutral line (Hoeksema and Scherrer, 1986; Hoeksema, 1991). Moreover, the neutral line can also be reconstructed from Hα heliograms,

in particular for years when direct observations were not yet available (McIntosh, 1979; Makarov and Sivaraman, 1989a, b; Obridko and Shelting, 1999).

All magnetic field components at any point in a spherical shell, extending from the photosphere to the so-called source surface, can be calculated under the potential field approximation from the observed longitudinal field in the photosphere. The source surface is, by definition, a sphere where all field lines are radial. It is generally placed at a distance $R_s \simeq 2.5\ R_\odot$ from the center of the Sun.

The equations used to calculate the magnetic field components are written as follows:

$$B_r = \sum P_1^m(\cos\vartheta)(g_{lm}\cos m\lambda + h_{lm}\sin m\lambda)\left((1+1)(R_0/R)^{l+1} - \right. \\ \left. -l(R/R_s)^{l-1}c_1\right)\ , \tag{1}$$

$$B_\vartheta = -\sum \frac{\partial P_l^m(\cos\vartheta)}{\partial\vartheta}(g_{lm}\cos m\lambda + h_{lm}\sin m\lambda)\left((R_0/R)^{l+2} + \right. \\ \left. +(R/R_s)^{l-1}c_l\right)\ , \tag{2}$$

$$B_\lambda = -\sum \frac{m}{\sin\vartheta} p_l^m(\cos\vartheta)(h_{lm}\cos m\lambda - g_{lm}\sin m\lambda)\left((R_0/R)^{l+2} + \right. \\ \left. +(R/R_s)^{l-1}c_l\right)\ . \tag{3}$$

Here, $0 \le m \le l < N$ (conventionally $N = 9$), $c_l = -(R_0/R_s)^{l+2}$, P_l^m is the Legendre polynomial, g_{lm} and h_{lm} are the coefficients of the spherical harmonic analysis based on the original observational data. These coefficients were tabulated by Hoeksema and Scherrer (1986) and Hoeksema (1991) for the time interval from May 1976 till January 1991. For earlier and later periods, they were directly calculated from the data that we received from T. Hoeksema and J. Stenflo.

A new sophisticated software package has been developed. It yields the synoptic charts of the source surface field, the maps of the original and the calculated line-of-sight fields on the photosphere surface, and the difference between the two maps. Synoptic charts of the radial, tangential, latitudinal, transverse, and line-of-sight components can be calculated for any height. The tangential field can be represented either as isocontours, or as vectors with a length proportional to the field intensity. Any date from 1965–1996 can be chosen as the center of the synoptic map.

At the next stage, the field line at every point on the map is analyzed to find out whether it is open (i.e., reaches the source surface) or closed (i.e., returns to its original height). For this purpose, the following procedure is applied. Choose a 'test level' in the solar atmosphere between 1.00 and 2.50 R_0. Starting from the source surface, where the field lines are open by definition and the grid points are evenly spaced, we trace every field line down to the chosen height, and find the coordinates of that point. The 'ends' of the field lines at that level will not be evenly spaced, but will rather be clustered to determine the 'open configuration' regions.

The density of the points at the test level will reveal the typical 'super-radiality' of coronal holes.

The potential approximation is probably quite reasonable, because we deal with a large-scale stationary magnetic field, and use only low spatial resolution data. Of course, the quantitative field characteristics calculated under the potential approximation may differ somewhat from the real ones, but the qualitative coupling of the computed OFRs and CHs is revealed quite satisfactorily (Altschuler, Trotter, and Orrall, 1972; Levine *et al.*, 1977; Pneuman, Hansen, and Hansen, 1978).

The neutral line on the source surface is the base of the of Heliospheric Current Sheet (HCS). As noted above, the HCS is not directly observed on the Sun, but can be calculated under potential approximation. However, its section by the ecliptic plane – the sector structure of the interplanetary magnetic field (SS IMF) – can be observed at the Earth orbit (King, 1979) or can be reconstructed from geomagnetic observations by the Mansurov-Svalgaard method (Mansurov, Mansurov, and Mansurova, 1976; Svalgaard, 1973, 1975). These values are regularly published in *Solar Geophysical Data*. Thus, we can compare with the directly observed structure.

Another remark is that only the lower harmonics, $l = 1, 2, 3$ contribute significantly to the calculated source surface field. Thus, proceeding to calculation at the source surface is similar to spatial filtration, when only the global magnetic field remains.

Some additional remarks concerning the magnetic field structure in the vicinity of coronal holes arise when comparing CHs localization with the high-speed streams of the solar wind.

The onset and duration of the high-speed solar wind streams were taken from the catalogues by Lindblad and Lundstedt (1981, 1983, 1989). For the onset we chose the moment when the solar wind velocity, averaged over 3 hours, increased more than by 100 km s^{-1} for a day. The end of HSWS was determined as the moment when the velocity recovered its original value or when a new HSWS started. The HSWS events associated with solar flares were excluded from consideration.

3. Magnetic Field Structure in Coronal Holes

Wang, Hawley, and Sheeley (1996) identified coronal holes with the open field regions and used the two terms interchangeably. However, the situation is not that simple. Even the latest calculations do not reveal the complete identity of these phenomena (Stepanyan, 1995; Mogilevsky, Obridko, and Shilova, 1997; Ioshpa, Mogilevsky, and Obridko, 1998; Obridko, 1998). The relationship between CHs and OFRs, which is well understood in principle, still involves some unclear points. In particular, Stepanyan (1995) noted a discrepancy between the spatial distributions of CHs and LSMF (background magnetic fields) over a solar cycle, which might indicate different origins. Comparison of a large number of open field con-

figurations with the coronal holes observed in X-ray and EUV bands on *Yohkoh*, SOHO, and CORONAS, as well as with the ground-based observations in He I 10830 (Obridko, 1998; Mogilevsky, Obridko, and Shilova, 1997) shows that OFRs are usually associated with CHs: there are CHs near and around OFRs and, vice versa, pronounced OFRs are usually recorded inside CHs. In this sense, OFRs are really good indicators of CHs, and following Wang, Hawley, and Sheeley (1996), we shall consider the two terms interchangeable for the purposes of *statistical* analysis. Unfortunately, this is not the case where detailed *physical* studies are concerned, because OFRs and CHs practically never coincide in space. This is not due to a calculation error. As stated earlier, our approximation gives an adequate description of the large-scale magnetic field of the Sun. The precise photometric boundaries of a coronal hole is not well defined in itself, particularly when observations are made in the lines of the transition zone and in He I 10830. It is obvious that the primary factor leading to the occurrence of coronal holes is a specific structure of the large-scale magnetic field. However, the contrast and photometric characteristics of CHs are also determined by the particular mechanisms of energy transport and release, that do not depend on the magnetic parameters alone.

Note that by statistical relationship between the calculated OFRs and CHs we mean first of all the coincidence of their centers of gravity. A full coincidence of the objects, including the coincidence of their boundaries is practically never observed. Besides, the very notion of CH boundary is quite uncertain, depending both on observation conditions, and on the assumed contrast at the boundary.

We should emphasize again that all OFRs, discussed below, are calculated, rather than directly observed.

Obridko and Shelting (1987a, b, 1988a, b, 1989, 1990) analyzed the relative position of the coronal holes, LSMF, source-surface magnetic field, and the projection of SS IMF and HSWS onto the solar surface. Coronal holes usually occur in extended unipolar regions of LSMF. If we filter out the local fields and consider only the global field with a characteristic size of the order of one solar radius (i.e., 2 or 3 low harmonics in Equations (1–3)), we shall see that coronal holes are not located over the weak fields, as is commonly supposed, but on the contrary, over the local maxima or hills of the global field. This naturally results from CH location in the unipolar zones of LSMF. CHs are usually observed inside the typical bends of the corrugated current sheet, making the latter depart from the equatorial zone. Since a characteristic structure of SS IMF is the 4-sector structure, we can often observe CHs spaced by 90° and arranged in pairs with the opposite field polarity in them.

The high-speed streams are undoubtedly related to the coronal holes and SS IMF boundaries (Obridko and Shelting (1987a, b, 1988a, 1989, 1990). However, they cover a much greater area than CHs, observed in X-rays or He I 10830 A. The east border of the HSWS is located in a transition zone 40–50° wide between the CHs and the SS IMF boundary. From 75 to 90% of the HSWS east borders are at a distance of 25–30° westward of SS IMF. Sometimes, the stream is recorded one

rotation before the coronal hole appears and persists for 1 or 2 rotations after its decay. Variations in the CH size or configuration often result in the enhancement of HSWS (Obridko and Shelting, 1987a, b, 1988a, 1989, 1990).

An interesting case was described by Ioshpa, Mogilevsky, and Obridko (1998). In the coronal hole, observed in the southern hemisphere in August 1996, only some of the calculated field lines were actually open. Many lines formed giant loops, that extended up to 1–1.3 solar radii and connected the CH with the north pole. It should be noted that such loops closely resemble open configurations, and the uncertainties of calculations are very large for them. Nevertheless, the hole under consideration had a contrast much lower than the 'typical' CH observed on the same days in the northern hemisphere.

In the recent years it has become clear that, besides the open configuration of the global magnetic field, another condition for the occurrence of coronal holes at mid-latitudes was the presence of active regions (AR) with strong local fields, in the vicinity. The relationship between CHs and AR was established in early work, based on the *Skylab* data (Levine, 1977). Wang *et al.* (1988) and Wang, Yoshimura, and Kundu (1988) also arrived at the conclusion that the formation of the open CH field was usually associated with the formation of two closed systems of field lines. Later on, it was shown (Shibata, Yokoyama, and Shimojo, 1994; Mogilevsky, 1995) that sometimes changes of boundaries and the energy balance in CHs were determined to a large extent by the sporadic and impulsive streams of hot ($T \approx 10^6$ K) plasma (X-ray 'jets') and the regular energy fluxes in the ambient AR field, as well as by the diffusion of X-ray 'points' through the CH boundaries. An active region in the vicinity of the coronal hole can be coupled with the latter via dynamics or energy (Mogilevsky, Obridko, and Shilova, 1997; Obridko, 1998). This coupling is likely to favor the escape of high-speed plasma streams from the coronal hole. A specific divergent pattern of the transverse component of the large-scale magnetic field sometimes transforms to a typical 'saddle' structure near the CH.

4. On the 'Coronal Hole – Sunspot Analogy'. Discussion of Some Earlier Results

It is generally accepted that coronal holes display 'super-radial' expansion (Kovalenko, 1983; Wang and Sheeley, 1990; Wang, Sheeley, and Nash, 1990), i.e., the field lines in these regions depart far from the radial direction, typical of the magnetic monopole. This is due to the fact that the field lines on the entire source surface originate in open field configurations connected with the coronal holes that cover only a small area in the lower corona and chromosphere. However, the situation here is not as simple, either. The super-radial expansion in the central part of the large coronal holes actually begins at about 1.4 solar radii from the center

of the Sun. Below this altitude, the field is strictly *radial*, unlike the surrounding closed field regions (Mogilevsky, Obridko, and Shilova, 1997; Obridko, 1998).

Thus, we adopt a scheme similar to that proposed by Wang, Yoshimura, and Kundu (1988) to account for radio observations of CHs and represented in Figure 2 in their paper.

The region between the closed field configurations is occupied by an open magnetic field (OFRs). At the center of OFRs up to the heights of 0.4–0.6 solar radii, there is a radial field region (RFR), that is what we observe as coronal hole in X-rays, EUV and He I 10830 A (Mogilevsky, Obridko, and Shilova, 1997; Obridko, 1998). In this region, enhanced radio emission is recorded in the meter and decameter wavelength ranges (Wang, Yoshimura, and Kundu, 1988). At the periphery of OFRs, in the vicinity of the closed field, one can observe over-radial expansion and thus, we have two OFR zones up to the altitude of 0.4 solar radii – the central RFR and the peripheral transition zone.

As shown by our calculations, the number of closed field lines in most active regions under consideration decreases abruptly in the vicinity of coronal holes at a distance above 1.4 R_o from the center of the Sun. This fact agrees with the typical dimensions of active regions. Of course, a certain number of very high loops exist anyway. Above, we have mentioned the field lines connecting the southern active region with the north pole (Ioshpa, Mogilevsky, and Obridko, 1998). However, on the whole, the interaction of closed fields with the ambient OFR regions at 1.4–1.7 R_o decreases.

These conclusions are invalid for minor coronal holes.

This scheme suggests a close analogy between sunspots (as observed in the photosphere) and coronal holes (Obridko and Shelting, 1989; Obridko, 1998). The main point is that a sunspot occurs in the context of a local magnetic field region, whereas a coronal hole is a similar-type object in the context of the large-scale magnetic field.

The features that are common to sunspots and coronal holes are as follows:

(a) Location at magnetic hills.

(b) Deficit of shorter wavelength radiation in the respective region (the optical emission from the photosphere for sunspots and EUV and X-ray emission from the lower corona for CHs), coupled with enhanced brightness at the heights of radio emission.

(c) Vertical field configuration at the center that gives way to rapid expansion at a certain height.

(d) Two zones (analogous to the umbra and penumbra of the sunspot) (Wang, Yoshimura, and Kundu, 1988; Mogilevsky, Obridko, and Shilova, 1997; Obridko, 1998). It is interesting to note that starting at some height, the rapid expansion of the field lines is determined by a sudden drop of the ambient density. In the case of CHs, a similar effect arises at a certain height due to disappearance of the system of closed field lines around it.

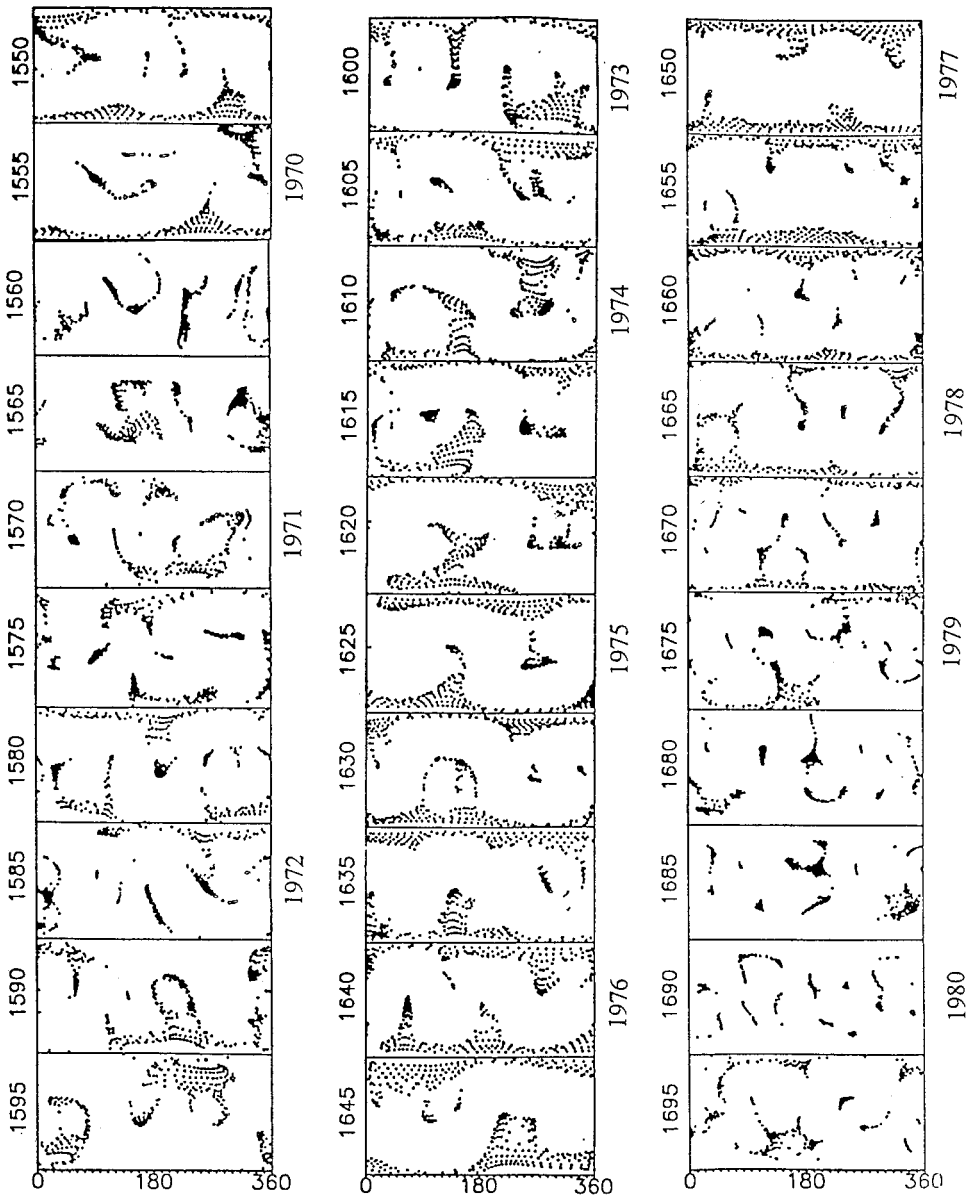

Figure 1a.

Figure 1. OFR synoptic maps for CR 1550–1915. Carrington rotations are indicated on the left of each panel. For some panels, the years are indicated on the right.

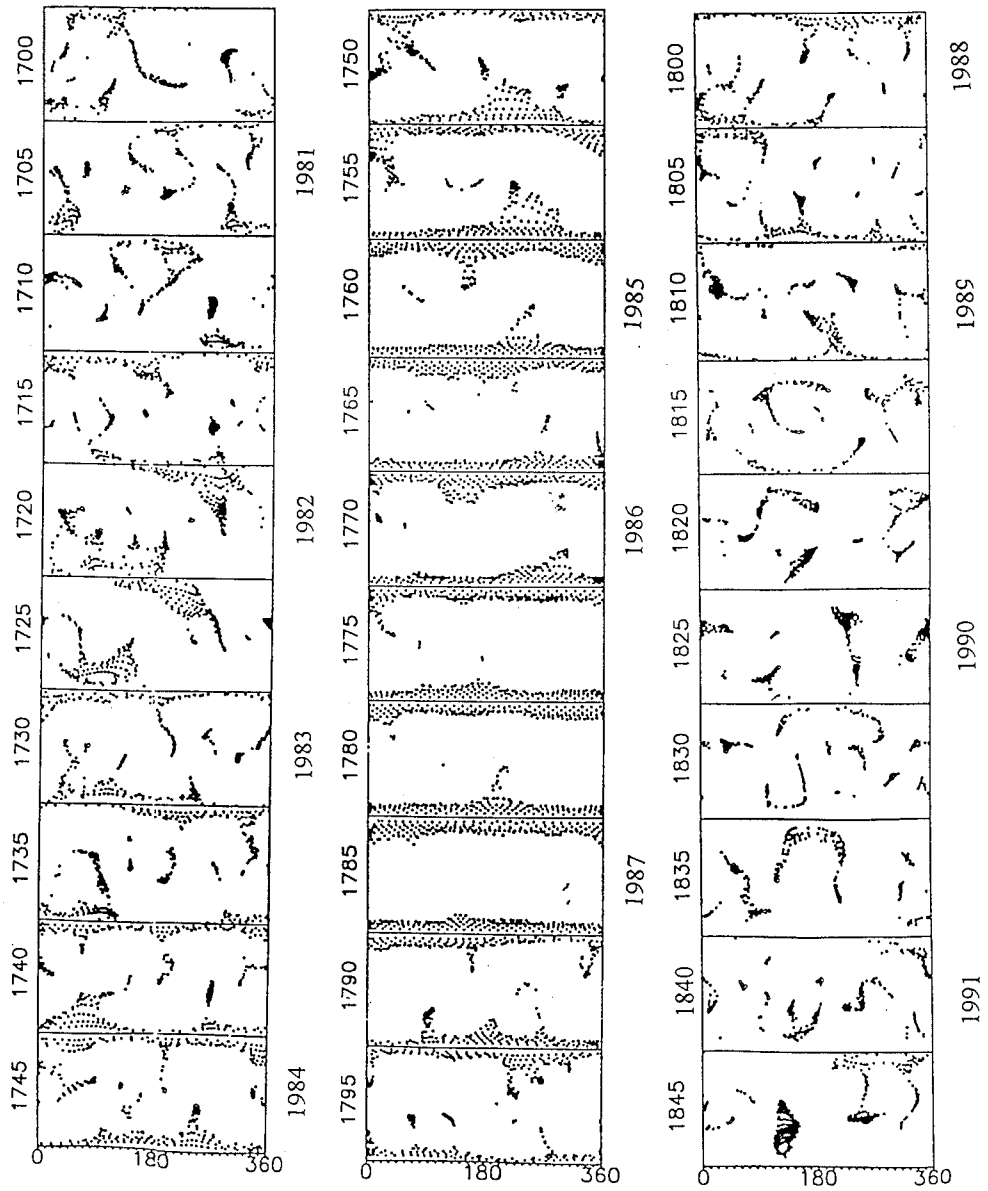

Figure 1b.

(e) Convergent transverse field in the immediate vicinity of sunspots and CHs (see figures in Mogilevsky, Obridko, and Shilova, 1997; Obridko, 1998).

(f) Strong matter outflow (at the photospheric level in the case of sunspots and in the lower corona in the case of CHs). In the photosphere, one can see an outflow along the field lines of the penumbra – the Evershed effect, which changes to inflow

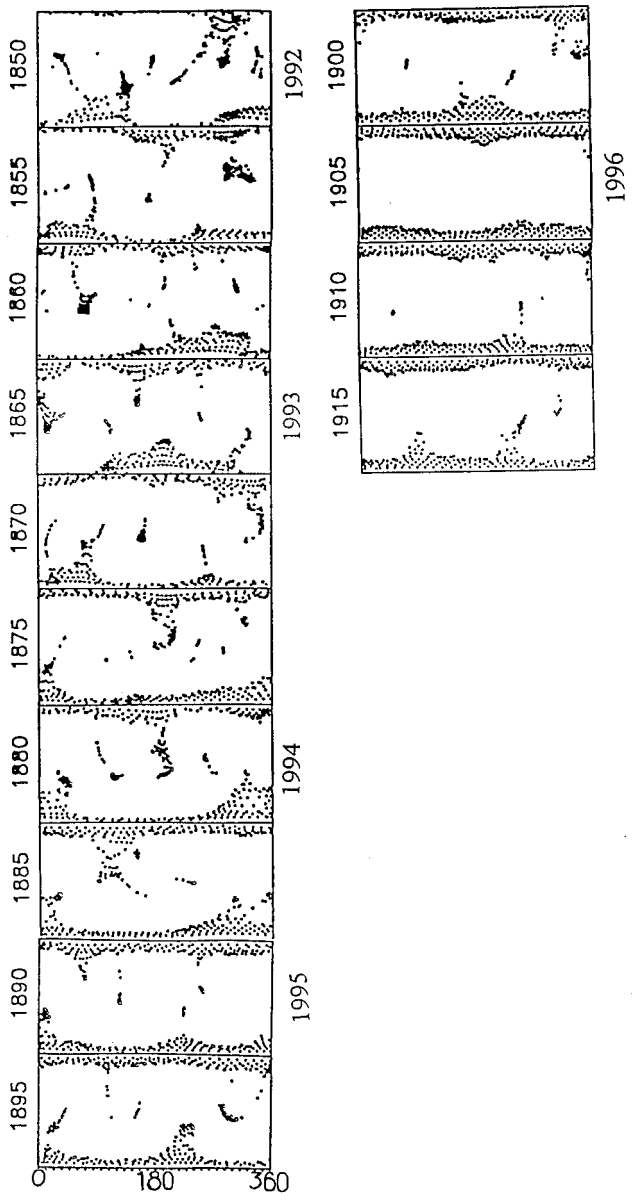

Figure 1c.

at the chromospheric level. The mass outflow along the field lines is also observed in coronal holes – HSWS.

(g) Sunspots usually join together to form bipolar groups. A similar effect was revealed in coronal holes. We often see two CHs, shifted about one another by $\sim 180^\circ$ in longitude. The magnetic fields in these CHs are opposite in sign and

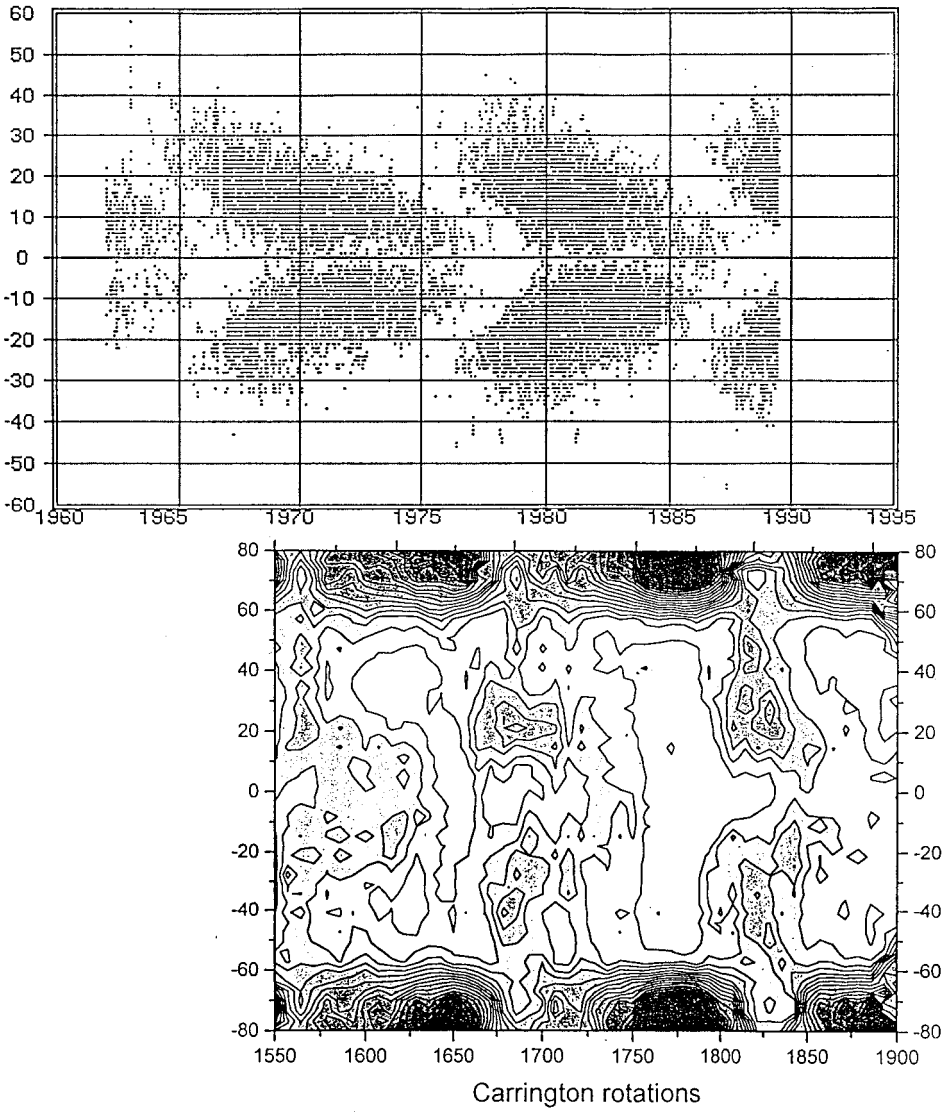

Figure 2. 'Butterfly' diagram of the open field. The lower panel represents the ratio of the open to the total flux and the upper panel the location of sunspots as a function of latitude and time.

are connected by a bridge with the solar poles. Such configuration is usually a manifestation of the 2- or 4-sector structure, and the coronal holes are located at the opposite bends of the heliospheric current sheet.

Of course, there cannot be full analogy. First, the typical dimensions of these objects differ by a factor of 10–30. Second, they exist at different levels in the solar atmosphere: sunspots – in the photosphere, and coronal holes – in the corona. Nevertheless, the primary physical phenomenon in both cases is the same, i.e.,

TABLE I

Cycle	t_{min}	t_{mA}	t_{AM}	t_{max}	t_{MD}	t_{Dm}
20					CR1560	CR1615
					04.1970	05.1974
21	CR1642	CR1660	CR1680	CR1690	CR1714	CR1750
	05.1976	09.1977	03.1979	12.1979	10.1981	01.1984
22	CR1778	CR1800	CR1813	CR1820	CR1840	CR1875
	07.1986	03.1988	03.1989	09.1989	03.1991	10.1993

a strong quasi-radial magnetic field. This means that one may expect a quasi-hydrostatic equilibrium along the axis. The processes of wave energy transport in these objects, as well as some other MHD processes are also likely to be similar. Future research will show whether it is the similarity or the distinction that prevails.

5. OFR Distribution on the Sun as a Function of the Solar Cycle

The whole magnetic field of the heliosphere originates in the open field regions on the Sun (OFRs) that occupy but a small part of the solar surface. Figure 1 indicates the feet of the open field lines calculated for the time interval from CR 1550 (14 July 1969) to CR 1915 (16 October 1996).

The OFR distribution on the solar disk changes sharply with the phase of the solar cycle. At the minimum of the cycle (CR 1615–CR 1660 and CR 1750–CR 1800) one can see the connected regions at the poles. At the maxima (CR 1680 –CR 1714 and CR 1813–CR 1840) the footpoints of the field lines form isolated small strips and cells. The change from one distribution pattern to another occurs over relatively short time intervals, usually coinciding with the reference points of the 11-year cycle, (introduced in Vitinsky, Kuklin, and Obridko, 1986; Obridko and Shelting, 1992; Obridko and Kuklin, 1993; Ivanov, 1995, 1996; Ivanov, Obridko, and Shelting, 1997). The reference points are the moments when all evolutionary processes of the solar cycle accelerate, and as such, they can be considered the basis of the cycle scenario. The main reference points during the time interval under consideration are listed in Table I.

Now, turning back to Figure 1 and comparing it with Table I, we can see that the evolution of OFRs is also connected with the reference points. At the end of the solar minimum, when the activity begins to grow (reference point t_{mA}), narrow streams and patches of open field configuration emerge from the simply connected polar OFRs and stretch to the equator. The polar region breaks down, but still exists up to the beginning of the maximum epoch (reference point t_{AM}), after which it vanishes rapidly. Then, during the whole phase of maximum up to t_{MD}, the open

field regions have the form of narrow streams or crooked paths. In some cases, OFRs are seen to form cells with a typical size of 60–90°. These cells have also been revealed in other work (Bumba *et al.*, 1968; McIntosh and Wilson, 1985; Ivanov, 1986, 1995, 1996). After the maximum phase is over, more or less simply connected regions of open field appear, but they do not completely cover the polar zone. This process coincides with reference point t_{Dm}, and signifies the beginning of the sunspot minimum.

It should be emphasized once more that, in our method (see Section 2 above), the points in Figure 1 are the feet of the field lines, which take their origin at the source surface at the evenly spaced points of the grid, and therefore do not depend on the magnetic field strength.

Earlier, Obridko and Shelting (1992) studied separately the cyclic behaviour of the total magnetic field and the source surface field (i.e., an open magnetic field). Here, we consider the ratio of the open flux to the total flux. In Figure 2, this ratio is represented as a function latitude and time. The plot was obtained as follows. First, we calculated the OFR flux value for each rotation, within a zone of 15° in latitude and 360° in longitude in the photosphere. This partial flux was divided by the total flux for the same relation. The total flux is the sum of the absolute values of fluxes of different sign, calculated in the photosphere. In Figure 2, this diagram appears together with the standard butterfly diagram for sunspots. One can readily see that the partial flux is the greatest at the growth and the maximum of the Wolf number cycle at mid-latitudes and at the minimum of the cycle – in the polar zones, where it reaches 100%. The polar and mid-latitude zones in each hemisphere are connected by narrow bridges.

When superimposed on the butterfly diagram of sunspots (Figure 3), the partial OFR fluxes display mid-latitude and equatorial branches that do not entirely overlap the butterfly pattern, but which are contiguous with it. This result is consistent with the conclusion, made in Section 3, of a close relationship between mid-latitude coronal holes and active regions or decaying AR flux (see also Wang *et al.*, 1988; Mogilevsky, Obridko, and Shilova, 1997; Obridko, 1998).

6. OFR Rotation

Using the locations of OFRs calculated for each rotation, we can determine their rotation velocity and compare it with the Carrington velocity. For this purpose, we identified all OFRs, that persisted during 4 rotations or longer, for each interval of 10 Carrington rotations. Then, the shift in OFR center of gravity longitude was determined for every rotation and converted into the effective rotation rate in deg day^{-1}. Figure 4 illustrates a diagram of sidereal angular velocity in degrees per day, vs. latitude, averaged for the entire time span of OFR data (solid line) and the law of rotation based on sunspots (dashed line) (Newton and Nunn, 1951). Equations (4a) and (4b) yield approximations of OFR rotation of the second and

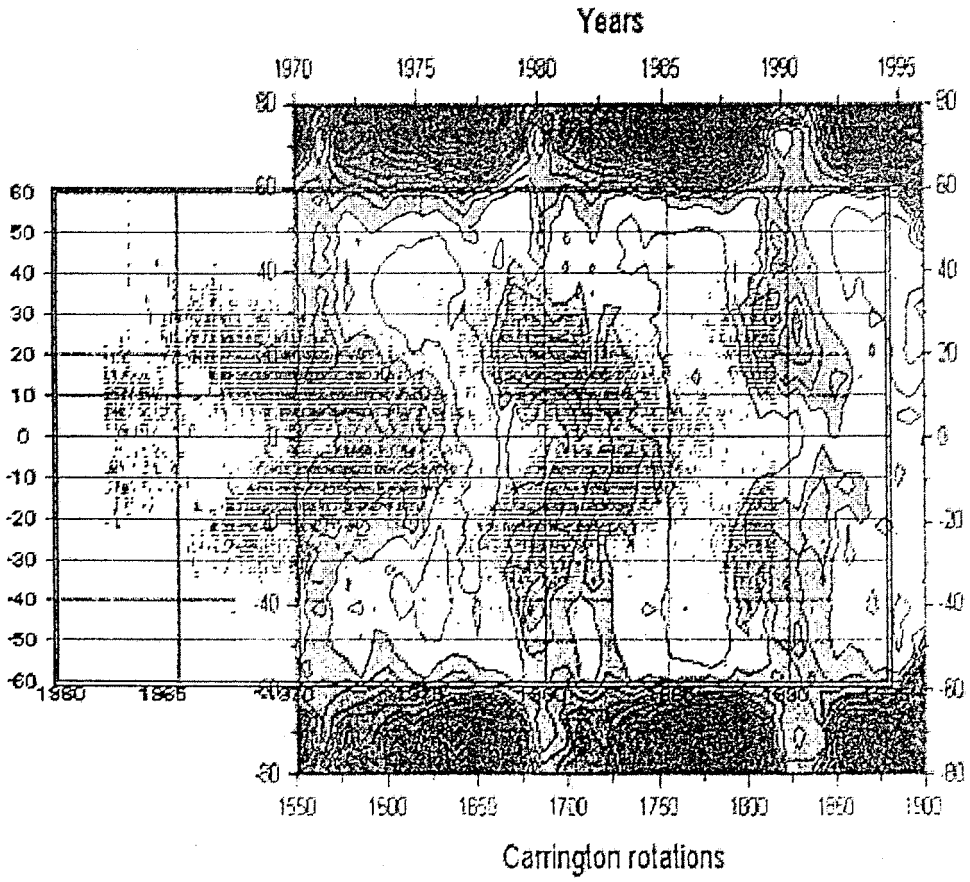

Figure 3. Overlapped 'butterfly' diagrams for the open fields and sunspots, taken from Figure 2.

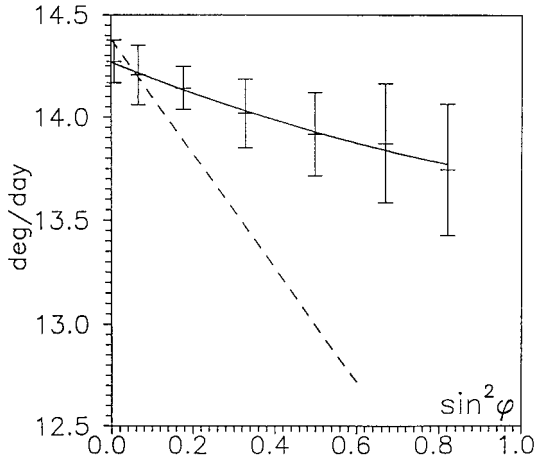

Figure 4. OFRs (solid line) and sunspot (broken line) rotation laws.

first order in $\sin^2 \varphi$, where $\varphi = 90^\circ - \theta$ is the latitude, and sunspot rotation law (Equation (4c)) for comparison:

$$V_{\text{sider}} = 14.268 - 0..796 \sin^2 \varphi + 0.236 \sin^4 \varphi \,, \tag{4a}$$

$$V_{\text{sider}} = 14.249 - 0.612 \sin^2 \varphi \,, \tag{4b}$$

$$V_{\text{sider}} = 14.38 - 2.77 \sin^2 \varphi \,. \tag{4c}$$

Figure 4 illustrates our calculations together with the r.m.s. error. Besides, it shows a curve (4a) and a straight line (4c). Within the limits of line thickness, (4b) does not differ from (4a).

Open field regions rotate much more rigidly than sunspots (Newton and Nunn, 1951; see also other determinations in Allen, 1973) and even more rigidly than the photospheric magnetic field (Snodgrass, 1983). Expression (5) is given to describe the measurements of Snodgrass. The numerical values from the original formula are converted from microrad s^{-1} to deg day^{-1}:

$$V_{\text{sider}} = 14.367 - 2.297 \sin^2 \varphi - 1.624 \sin^4 \varphi \,. \tag{5}$$

The rigid rotation of OFRs is just what should be expected because OFRs are closely connected with coronal holes, for which this effect is well known. In binomial representation ($V = a + b \sin^2 \varphi$), Timothy, Krieger, and Vaiana (1975) obtained $b = -0.4$ for the time interval of November 1972 to August 1973, Wagner (1975) obtained $b = -0.39$ for the time interval of May 1972 to October 1973, and Obridko and Shelting (1988b, 1989) obtained $b = -1.04$ for 1978–1984, and $b = -0.44$ for 1985. This is probably due to the fact that both OFRs and CHs manifest a global (lowest orders of space harmonics) activity of the Sun, which originates deep in the solar interior.

Figure 5 shows the rotation velocity of OFRs at the equator as a function of time and Figure 6 represents the second coefficient in the binomial Equation (4b). R.m.s. errors are shown in the figures. It is difficult to say whether a sudden decrease in equatorial rotation velocity soon after cycle minimum in the growth phase and at the maximum of cycle 22, is typical. At least, this effect is absent at the growth phase of cycle 21. However, it should be noted that the data for cycle 21 were not obtained with the same magnetograph and, therefore, may have some systematic differences. From the formal point of view, the r.m.s. error at these points is small enough. One might suggest that the decreasing rotation rate at the equator is merely due to the small number of OFRs, observed in the equatorial zone in the minimum epoch. However, the fact is that the rotation rate at the very minimum does not differ much from its value at the maximum of the cycle, whereas a deceleration is recorded in the growth phase, when the appearance of OFRs is frequent enough.

It appears that rotation at the minimum is more rigid than at the growth phase and the maximum of the cycle, which seems to be due to the influence of local fields.

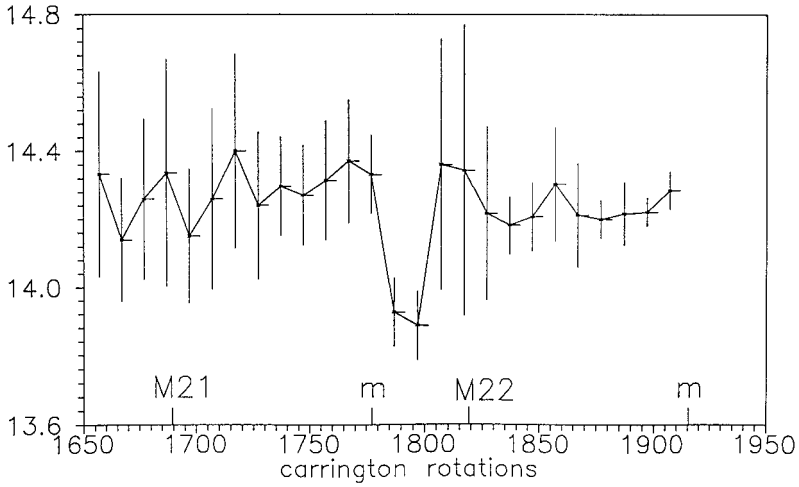

Figure 5. Angular sidereal rotation velocity of OFRs at the equator as a function of time, expressed in Carrington rotations. Maxima of the cycle 22 (CR1820) and cycle 21 (CR1690) and minima (CR1778 and CR1910) are marked below. See Table I.

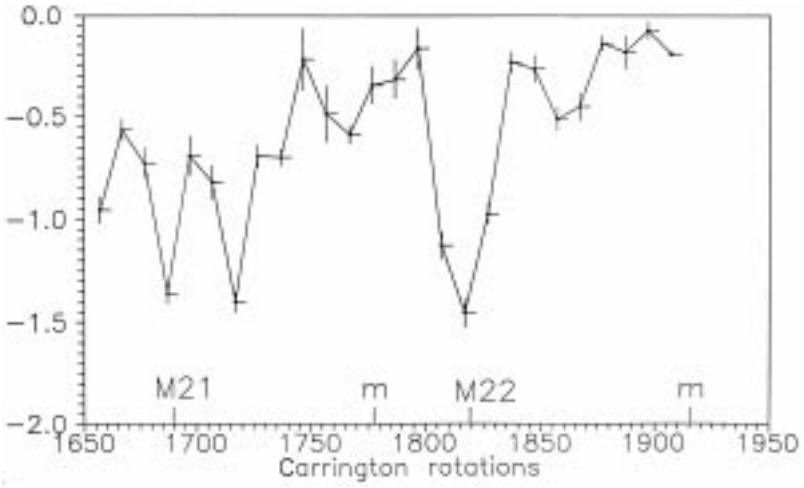

Figure 6. The degree of differentiality of OFR rotation (second coefficient in a binomial equation of (4b) type) as a function of time. Maxima of cycle 22 (CR1820) and cycle 21 (CR1690) and minima (CR1778 and CR1910) are marked below. See Table I.

Figure 7 illustrates the difference between the local angular velocity of OFRs and the average angular velocity over the entire interval under investigation (4a). This difference ranges from -0.6 deg day^{-1} to 0.8 deg day^{-1}. The positive values in the figure are shown with solid lines and the negative values – with dashes. Isolines are drawn in every 0.05 deg day^{-1}.

Until rotation 1778 (i.e., the minimum of cycle 22), the acceleration and deceleration of OFRs agrees on the whole with the data, obtained by Antonucci,

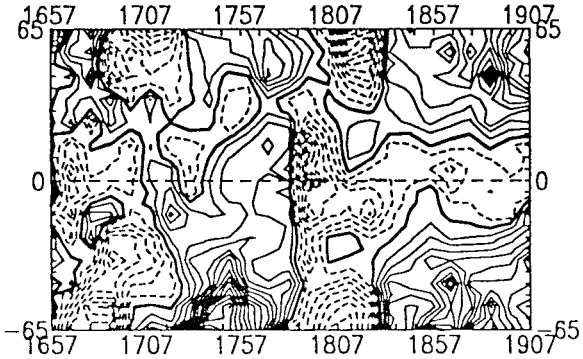

Figure 7. Acceleration and deceleration of OFRs. The values range from -0.6 deg day^{-1} to 0.8 deg day^{-1}. The positive values are shown with solid lines, the negative values with dashes. Isolines are drawn in every 0.05 deg day^{-1}.

Hoeksema, and Scherrer (1990) from the analysis of the photospheric magnetic field until 1985. Then, in the growth and maximum phases, the deceleration is observed almost simultaneously at all latitudes. This effect does not resemble torsional oscillations. It can rather be stated that the entire OFR system at all latitudes accelerates before the minimum and decelerates in the growth phase and at the maximum of the cycle. Since an abrupt deceleration occurs at all latitudes, lasts from the minimum to the maximum of the cycle, and is large enough to exceed the errors in Figures 5 and 6, we believe it to be a real phenomenon, and not being associated with a small number of observed OFRs in the periods under consideration. Nevertheless, this result seems so surprising that it should to be verified by other methods.

7. Some Particular Features in Cyclic Evolution of the Global Field

To study the long-term evolution of the open field regions, we construct a diagram, consisting of multi-latitude stack plots. From each synoptic map with the feet of the open field lines plotted on it (see Figure 1) we cut out a strip, corresponding to a given latitude and then we arrange the strips one over another. This method is similar to that of Wang, Yoshimura, and Kundu (1988), McIntosh (1992), Bumba, Klvaňa, and Sýkora (1995), and our Figure 8 is on the whole similar to Figure 2(b) in the paper by Wang, Yoshimura, and Kundu (1988). It this paper, we have considered a longer time interval. It allowed us to form a reliable judgment of more than two solar cycles and to observe two cases of sign reversal.

Two effects are to be noted in Figure 8. In the vicinity of the 11-year maxima, the sign reversal takes place in all OFRs and is practically simultaneous at all latitudes. The sign reversal (SR) at the end of 1979 occurred almost simultaneously in the northern and southern polar regions and took only a few solar rotations. SR

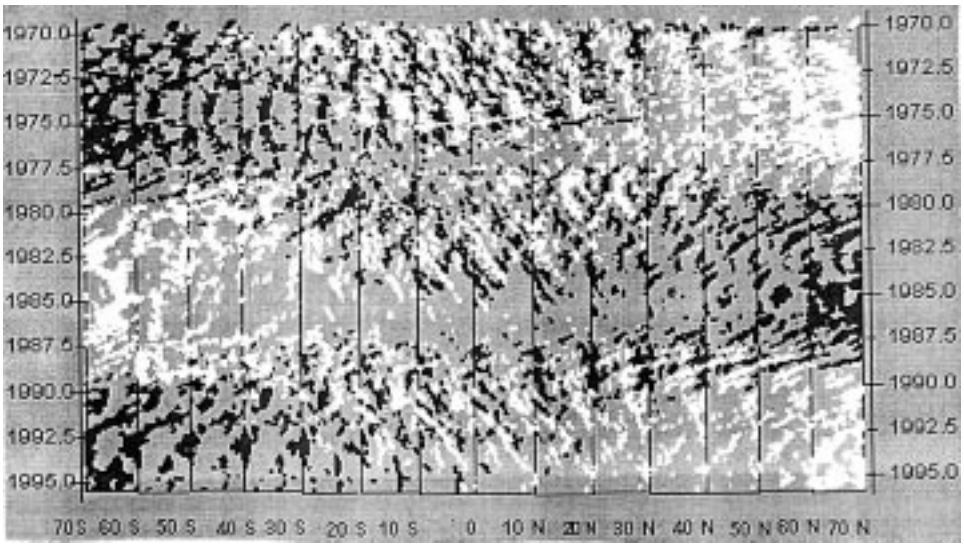

Figure 8. Time-latitude diagram for OFRs.

in the mid- and low-latitude OFR occurred in the same 1979, but lasted longer. SR at high latitudes in the following cycle took place at the end of 1989 in the northern hemisphere and a few months later in the southern hemisphere. SR at lower latitudes occurred approximately at the same time, but again it was slower. This implies that an OFR behaves as an integral object, changing its polarity over a few months. The truth is that after keen examination, the figure displays a somewhat curved 'field reversal line' in 1979. It means that the polarity of the open field at the equator changed some months earlier than at the pole. Nevertheless, this time delay is negligible as compared to the length of the cycle. The situation is quite different when we do not divide the solar magnetic field into the local and global components. The integral magnetic field changes its polarity at the equator at the minimum of the cycle, i.e., several years earlier than at the poles, where the sign reversal takes place in the epoch of solar maximum. The OFRs at all latitudes change sign rapidly at the maximum of the Wolf number solar cycle. Since field, observed in the heliosphere, is based on OFRs, we can draw the conclusion that it also changes the sign over a short interval at all latitudes; presumably as a result the change of polarity would propagate out with the solar wind.

The effect of quasi-simultaneous sign reversal of OFRs at all latitudes is, in the physical and computational aspect, a natural result of the fact that they form part of the large-scale magnetic field and are determined by its lowest harmonics. The reversal of the most powerful harmonic (the dipole) leads to a quick reversal of OFRs at all latitudes.

Another remark concerns the OFR rotation velocity. On the diagram in Figure 8, one sees two inter-threading fluxes, going down left and right. The simplest expla-

nation is that OFRs rotate at a velocity different from the Carrington reference frame. Figure 8 suggests that OFRs differ from the local fields, which display a gradual transition from the synodic periods of about 26.9 days on the equator to 30 and more days at high latitudes. The rotation of OFRs displays two typical periods, 26.8 and 28.0 days, which exist simultaneously at all latitudes. The same conclusion was made earlier by Ivanov (1986, 1995), Hoeksema (1989, 1991b), Antonucci, Hoeksema, and Scherrer (1990). As shown by Hoeksema and Scherrer (1987), the magnetic field in the corona (at the source surface) rotates with two fixed periods of 27 and 28 days all over solar cycle 21. Besides, Hoeksema and Scherrer (1987) noted an asymmetry in the rotation of both hemispheres: during 1976–1982, the northern hemisphere rotated faster (with a period of 27 days) than the southern hemisphere, where the period of 28 days was predominant. Then, up to 1985, both periods were equally pronounced in the northern and the southern hemispheres.

Our analysis covers the interval 1970–1995 and deals with the calculated OFR locations in the photosphere. Therefore, our results, which agree on the whole with Hoeksema and Scherrer (1987), display some difference in the interval of 1978–1982.

In Figure 8, the vertical strips correspond to the rotation period of 27.3 days, the strips going down right correspond to a faster rotation ($<$27 days), and the strips going down left to a slower rotation ($\cong$28 days). As seen from the Figure, all strips in the northern hemisphere (at $\varphi \geq -20^\circ$) go down to the right (i.e., the rotation period is $\leq$27) beginning with 1970, when the global field reversal takes place. In the southern hemisphere (especially at $\varphi \leq -20^\circ$), the rotation rate is lower (the rotation period is $\geq$28 days). This regime exists until the beginning of 1980 (i.e., until the maximum of the cycle and the global field reversal are recorded). After that, a rotation mode with a period of 28 days appears suddenly in the northern hemisphere. It increases gradually to become predominant. Though OFRs vanish for some time at the minimum of the cycle (1985), they reappear with the same rotation period of 28 days. In the southern hemisphere, on the contrary, the 28-day mode disappears soon and the period of 27 days is predominant. The zone of $\pm 20^\circ$ from the equator is the only one where both modes are present. This regime persists until 1990. Later on, one observes both modes in the northern hemisphere and preferably the 28-day mode in the southern hemisphere. All this gives the impression that the rotation period in both hemispheres changes in a cyclic fashion, and the rotation mode changes at the reversal of the global field.

Acknowledgements

The work was carried out under the sponsorship of the Russian Foundation for Basic Research, grant No. 96-02-17054. The authors are grateful to A. F. Kharshi-

ladze and I. V. Dmitrieva for the development of application programs. We are also grateful to the referee for valuable remarks.

References

Allen, C. W.: 1973. *Astrophysical Quantities*, The Athlone Press, University of London.
Altschuler, M. D., Trotter, D. E., and Orrall, F. Q.: 1972, *Solar Phys.* **26**, 354.
Antonucci, E., Hoeksema, J. T., and Scherrer, P. H.: 1990, *Astrophys. J.* **360**, 296.
Bumba, V.: 1970, *Solar Phys.* **14**, 80.
Bumba, V., Klvaňa, M., and Sýkora, J.: 1995, *Astron. Astrophys.* **298**, 923.
Bumba, V., Howard, R., Martres, M. J., and Soru-Iscovici, J.: 1968, 'Structure and Development of Solar Active Regions', *IAU Symp.* **35**, 13.
Hoeksema, J. T.: 1989, *Adv. Space Res.* **9**(4), 141.
Hoeksema, J. T.: 1991a, *Solar Magnetic Fields – 1985 through 1990*, Report CSSA-ASTRO-91-01.
Hoeksema, J. T.: 1991b, *Adv. Space Res.* **11**(1), 15.
Hoeksema, J. T. and Scherrer, P. H.: 1986, *Solar Magnetic Fields – 1976 through 1985*, WDCA, UAG Report 94, Boulder, USA.
Hoeksema, J. T. and Scherrer, P. H.: 1987, *Astrophys. J.* **318**, 428.
Ioshpa, B. A., Mogilevsky, E. I., and Obridko, V. N.: 1998, *New Perspectives on Solar Prominences*, IAU Colloquium 167, ASP Conference Series, Vol. **150**, p. 393.
Ivanov, E. V.: 1986, *Solnechnye Dannye* No. 61.
Ivanov, E. V.: 1995, *Izv. RAN* **7**, 29.
Ivanov, E. V.: 1996, *J. Geomag. Geoelectr.* **48**(1), 11.
Ivanov, E. V., Obridko, V. N., and Shelting B. D.: 1997, *Astron. J.* **74**, 273.
King, J. H.: 1979, *Interplanetary Medium Data Book*, NSSDC/NDCA, Goddard Space Flight Center, Greenbelt, Suppl. 1, 1975–1978, Suppl. 2, 1978–1982.
Kovalenko, V. V.: 1983, *Solar Wind*, Nauka, Moscow, p. 272.
Krieger, A. S., Timothy, A. F., and Roelof, E. C.: 1973, *Solar Phys.* **29**, 505.
Levine, R. H.: 1977, in J. B. Zirker (ed.), *Coronal Holes and High Speed Wind Streams*, Colorado Associated University Press, Boulder, p. 103.
Levine, R. H., Altschuler, M. D., Harvey, J. W., and Jackson, B. V.: 1977, *Astrophys. J.* **215**, 636.
Lindblad, B. A. and Lundstedt, H.: 1981, *Solar Phys.* **74**, 197.
Lindblad, B. A. and Lundstedt, H.: 1983, *Solar Phys.* **88**, 377.
Lindblad, B. A. and Lundstedt, H.: 1989, *Solar Phys.* **120**, 145.
Makarov, V. N. and Sivaraman, K. R.: 1989a, *Solar Phys.* **119**, 35.
Makarov, V. N. and Sivaraman, K. R.: 1989b, *Solar Phys.* **123**, 367.
Mansurov, S. M., Mansurov, G. S., and Mansurova, L. G.: 1976, Antarktika, No. 15, p. 16.
McIntosh, P. S.: 1979, *Annotated Atlas of the Hα Synoptic Charts for Solar Cycle 20 (1964–1974)*, Report UAG-70.
McIntosh, P. S.: 1992, in K. L. Harvey (ed.), *The Solar Cycle, ASP Conference Series, Proceedings of the NSO/SP 12th Summer Workshop*, p. 14.
McIntosh, P. S. and Wilson, P. R.: 1985, *Solar Phys.* **97**, 59.
Mogilevsky, E. I.: 1995, *Geomagn. Aeron.* **3**(6), 11.
Mogilevsky, E. I., Obridko, V. N., and Shilova, N. S.: 1997, *Solar Phys.* **176**, 107.
Munro, R. H. and Withbroe, G. L.: 1972, *Astrophys. J.* **176**, 511.
Newton, H. W. and Nunn, M. D.: 1951, Monthly Noties Royal Astron. Soc., **111**, 413.
Obridko, V. N.: 1998, Advances in Solar Connection with Interplanetary Phenomena, Proceedings of the Third SOLTIP Symposium, Beijing, China, October 14–18, 1996, Beijing, 1998, 41–48.

Obridko, V. N. and Kuklin, G. V.: 1993, in J. Hruška, M. A. Shea, D. F. Smart, and G. Heckman (eds.), *Solar-Terrestrial Predictions*, IV. Proc. Workshop at Ottawa, Canada, May 18–22, 1992, Vol. 2, p. 273.
Obridko, V. N. and Shelting, B. D.: 1987a, *Geomagn. Aeron.* **27**, 197.
Obridko, V. N. and Shelting, B. D.: 1987b, *Geomagn. Aeron.* **27**, 660.
Obridko, V. N. and Shelting, B. D.: 1988a, *Kinematika i fizika nebesnykh tel* **4**, 29.
Obridko, V. N. and Shelting, B. D.: 1988b, *Soln. Dannye* No. 1, 89.
Obridko, V. N. and Shelting, B. D.: 1989, *Solar Phys.* **124**, 73.
Obridko, V. N. and Shelting, B. D.: 1990, *Astron. Zh.* **67**, 890.
Obridko, V. N. and Shelting, B. D.: 1992, *Solar Phys.* **137**, 167.
Obridko, V. N. and Shelting, B. D.: 1999, *Solar Phys.* **184**, 187.
Obridko, V. N., Konstantinova, L. Yu., Konakh, M. M., and Mansurov, G. S.: 1986, *Geomagn. Aeron.* **26**, 313.
Pneuman, G. W., Hansen, S. F., and Hansen, R. T.: 1978, *Solar Phys.* **59**, 313.
Rozelot, J. P.: 1983, *Ann. Phys.* **8**, 539.
Sheeley, N. R., Harvey, J. W., and Feldman, W. C.: 1976, *Solar Phys.* **49**, 271.
Shibata, K., Yokoyama, T., and Shimojo, M.: 1994, in *Proceedings of Kofu Symposium*, NRO, p. 75.
Snodgrass, H. B.: 1983, *Astrophys. J.* **270**, 288.
Stepanyan, N. N.: 1995, *Izvestiya RAN, Phys. Ser.* **59**, 63.
Svalgaard, L.: 1973, *IAGA Bull.* No. 34, 401.
Svalgaard, L.: 1975, *Solar Phys.* **45**, 83.
Timothy, A. F., Krieger, A. S., Vaiana, G. S.: 1975, *Solar Phys.* **42**, 135.
Veselovsky, I. S.: 1984, *Physics of Interplanetary Plasmas, Itogi nauki I tekhniki*, Series Space Research, Vol. **22**, VINITI, p. 140.
Vitinsky, Yu. I., Kuklin, G. V., and Obridko, V. N.: 1986, *Soln. Dannye* No. 3, 53.
Wagner, W. J.: 1975, *Astrophys. J.* **198**, L141.
Wang, Y.-M. and Sheeley, N. R., Jr.: 1990, *Astrophys. J.* **355**, 726.
Wang, Y.-M. and Sheeley, N. R., Jr.: 1992, *Astrophys. J.* **392**, 310.
Wang, Y.-M., Sheeley, N. R., Jr., and Nash, A. G.: 1990, *Nature* **347**, 439.
Wang, Y.-M., Hawley, S. H., and Sheeley, N. R., Jr.: 1996, Science **271**, 417.
Wang, Z., Yoshimura, H., and Kundu, M. R.: 1988, Solar and Stellar Structure and Dynamics, Proceedings of the Ninth Sacramento Peak Summer Symposium, Sunspot, NM, National Solar Observatory, p. 458.
Wang, Z., Kundu, M. R., Yoshimura, H., and Hathaway, D. H.: 1988, in Proceedings of STIP Symposium on Physical Interpretation of Solar/Interplanetary and Cometary Intervals.
Withbroe, G., Wang, Y.-M.: 1972, *Solar Phys.* **27**, 394.